symmetry

MDPI

Article

Effects of Nanoparticle Enhanced Lubricant Films in Thermal Design of Plain Journal Bearings at High Reynolds Numbers

Mohammad Yaghoub Abdollahzadeh Jamalabadi [1,2,*], Rezvan Alamian [3], Wei-Mon Yan [4], Larry K. B. Li [5], Sébastien Leveneur [6] and Mostafa Safdari Shadloo [7]

1 Department for Management of Science and Technology Development, Ton Duc Thang University, Ho Chi Minh City 700000, Vietnam
2 Faculty of Civil Engineering, Ton Duc Thang University, Ho Chi Minh City 700000, Vietnam
3 Sea-Based Energy Research Group, Babol Noshirvani University of Technology, Babol 47148, Iran; ralamian@nit.ac.ir
4 Department of Energy and Refrigerating Air-Conditioning Engineering, National Taipei University of Technology, Taipei 10608, Taiwan; wmyan1234@gmail.com
5 Department of Mechanical and Aerospace Engineering, The Hong Kong University of Science and Technology, Clear Water Bay, Hong Kong; larryli@ust.hk
6 Normandy University, INSA of Rouen, LSPC, EA4704, 76000 Rouen, France; sebastien.leveneur@insa-rouen.fr
7 CORIA Lab./CNRS (UMR-6614), University and INSA of Rouen, Normandie University, 76000 Rouen, France; msshadloo@coria.fr
* Correspondence: abdollahzadeh@tdtu.edu.vn

Received: 5 October 2019; Accepted: 30 October 2019; Published: 1 November 2019

Abstract: Performance investigation of oil journal bearings is of particular importance given the growing use of them as a support for rotary components in a wide range of industrial machines. Frictional forces and shear stresses, which are proportionate to the velocity of lubricating layers at different points in the bearing space, provide the basis for changing temperature conditions. Various factors such as rotational velocity increase, slip width reduction, and small heat transfer coefficient of lubricant cause intensification of lubricant temperature changes. In the present study, with using computational fluid dynamic (CFD) thermohydrodynamic (THD) numerical simulations, the effect of nanoparticles on the performance features of plain journal bearings is evaluated. Particularly, 3D simulation of a journal bearing is implemented using CFD which considerably improves the accuracy of results, coupled with conjugate heat transfer model for metal parts of bearings. Reynolds equation model is used to calculate the oil-film pressure developed in hydrodynamic journal bearings by applying the nano-based lubricants. The configuration of thrust bearing consists of six pads in this study. In order to reduce the modeling complexity and computational cost and because of the symmetrical geometry of the pads, simulation of a single pad is considered instead of the entire domain. In this study, TiO_2 nanoparticle with different volume fraction percentages are used. The parameters that are changed to evaluate the performance of the bearing include volume fraction percentage of the nanoparticle, type of lubricant, and rotational speed. Based on the results, for all different lubricant types, the dissipation power, average shear stress, and temperature rise are increased with augmenting the rotational speed. By increasing the rotational speed from 500 to 1500 rpm, the average shear stress increases by more than 100%, 120%, and 130% for DTE 26, DTE 25, and DTE 24 lubricant types, respectively. Moreover, by increasing the rotational speed from 500 to 1500 rpm, the dissipation power, and temperature rise are increased around 600% and 800%, respectively. Furthermore, increasing nanoparticles volume fraction from 0% to 10%, increases all parameters by approximately 10% for all lubricant types and in all rotational speeds.

Keywords: thermodynamic analysis; journal bearing; viscous heating; nanofluids

1. Introduction

The main difference between machines and structures are moving parts such as bearings. In bearings, this movement is generally resisted by friction on machine joints, and the work required to sustain motion is largely converted to heat due to the shear generated between the static and dynamic parts. Such heat generation may lead to joint deformation, which can further impose defects on operational conditions including physical contact and freedom of movement. Thus, it is crucial to improve the performance of bearings to obtain higher workability from machines. This necessitates investigations on working conditions and the influence of different important parameters on bearings.

In journal bearings, factors such as high speed of rotor rotation, high friction between the lubricant layers and changing environmental conditions of the rotary system, including bearing, will cause significant changes in lubricant temperature. The relationship between applied forces and friction is well described in reference [1]. Excessive variation in temperature will lead to changes in various properties of the lubricant fluid, especially viscosity, and cause problems such as lubricant oxidation and deformation of the bearing and rotor shell. Considering that the effects of lubricant temperature variations and heat transfer currents formed between the rotor, lubricant, and shell on the static and dynamic performance of bearings can lead to more realistic results of journal bearing performance, research on this issue has grown significantly in the last decade.

For the present study, the heat transfer problem was treated at high Reynolds number [2]. This phenomena has been a subject of investigations for numerous studies [3]. In an earlier study for evaluating the effect of temperature variations on the lubrication of journal bearings, Crosby [4] investigated the thermohydrodynamic performance of circular journal bearings for certain specific situations. Nagaraju et al. [5] examined the thermal behavior of elliptical journal bearings and considered some of the static performance characteristics such as bearing load capacity, lateral leakage, friction force, and the attitude angle as well as some of the dynamic performance characteristics of bearing, such as critical mass and damped whirl frequency ratio. The thermal behavior of elliptical and axial groove bearings was studied by Ma and Taylor [6]. In this study, the researchers tested bearings under certain pressures up to 4 MPa and rotational frequency of 120 Hz and reported the effect of temperature on power loss and fluid direct flow rate. Their results indicated the significant influence of temperature variation on the bearing performance. Banwait and Chandrawat [7] analyzed the effect of rotor misalignment on the thermohydrodynamic performance of elliptical journal bearings. In their study, the generalized Reynolds equation for calculating pressure distribution in oil film, simultaneously with energy and heat transfer equations, is investigated to determine the temperature range in bush, journal, and oil film. The results of this study reveal the significant effect of temperature changes on the pressure distribution inside the lubricant fluid film.

Singh and Majumdar [8] carried out computer-aided simulations of circular hydrodynamic journal bearings considering thermal effects. By analyzing the Reynolds equation with energy and heat transfer equations, they investigated the steady-state performance of hydrodynamic journal bearings. Mishra et al. [9] examined the effect of temperature on elliptical journal bearing and compared the results with similar circular bearings. Their evaluation suggested that the effect of temperature variation on the performance of elliptical bearings is decreased by increasing the non-circularity of bearing; this occurred due to the simultaneous weakening of the amount of pressure created in the lubricant film inside the bearing. In another study, the thermohydrodynamic study of elliptical journal bearings with three different commercial oil types was performed by Chauhan et al. [10]. The purpose of this study was to investigate the increase in oil temperature, pressure changes due to heat exchange, and determination of bearing capacity in different states to specify the most suitable type of oil used. A combined effect of surface roughness, heat, and fluid inertia on the performance characteristics of

hydrodynamic journal bearings was investigated by Prasad et al. [11]. Singla et al. [12] investigated the effect of variations of temperature and viscosity of incompressible lubricant fluid on the performance of hydrodynamic circular journal bearings by means of numerical simulation in Ansys-Fluent software and three-dimensional flow assumption in the Reynolds equation. The results of this study indicated that reduction in the range of lubricant temperature changes before steady-state conditions was attained by considering the stepwise viscosity changes at each stage of the calculation compared to the isothermal assumption of lubricant fluid film.

As can be seen in the abovementioned articles, there has been numerous studies in literature to improve the performance and design of journal bearings by investigating the effect of different parameters [13]. In particular, the effect of additive nanoparticles is one of main research directions [14]. Nanofluids have recently received much attention due to numerous reports on the dramatic increase in thermal properties [15]. Nanoscience has been expanding ever since its birth. Due to their properties, nanomaterials have attracted the attention of scientists in various fields [16]. Nanoparticles have been used to improve the properties of many carrier fluids including coolants [17] and lubricants [18]. Due to their very small size, these particles are able to reach very fine points on the metal surface and thus improve the lubricating properties of the lubricants on the contact surfaces. Nanofluids derived from the distribution of nanoparticles in ordinary fluids are a new generation of highly potential fluids in industrial applications. The particle sizes used in nanofluids range from 1–100 nanometers. These particles are made of metal oxides, sulfides, carbon-based compounds, nano-diamonds, and other compounds [19]. It has been shown that adding specific percentage of different nanoparticles such as TiO_2, Al_2O_3, CuO, etc. can significantly influence several aspects of journal bearing performance such as thermodynamic characteristics and tribological performance [20].

Lee et al. reported the lubrication properties of graphite nano lubricants [21]. Their reports represent that lubricant-coated surfaces include graphite nanoparticles, have less friction coefficient and less wear compared to conventional lubricated surfaces. Preparation and evaluation of lubricants including aluminum nitride nanoparticles by Tao et al. [22] have been reported in 2014. An investigation of the load capacity of journal bearings by an oil lubricant including titanium oxide nanoparticles by the variable viscosity method has been reported by Binu et al. [23]. Their research demonstrated the increased load-bearing capacity of lubricated journal bearings with titanium oxide nanoparticles. The study of the static properties of lubricated bearings including titanium oxide nanoparticles is carried out by using the modified Krieger–Dougherty viscosity model and the couple stress model by Binu et al. [24]. Their studies showed that titanium oxide nanoparticles have a significant effect on improving the lubricant's load-bearing capacity. Babu et al. presented the analysis of lubricated journal bearings including aluminum oxide and zinc oxide nanoparticles [25]. Their results showed that increasing the amount of nanoparticles increases the viscosity of the lubricant, thereby changing the performance characteristics of the journal bearing. The effect of copper oxide nanoparticles as an additive on reducing friction and wear on lubricating oils was studied by Jatti and Singh [26]. Their results proved that nanoparticles can effectively enhance the lubrication properties of engine oils. The nanoparticles change the sliding friction to rotational friction, thereby reducing the effective friction coefficient.

Considering the above literature review, there is less attention paid towards the prediction of the oil-film pressure in hydrodynamic journal bearings to the best of the authors' knowledge. Moreover, the distribution of heat generation is not properly addressed for systems under the influence of nano-based lubricants. In present research, with using computational fluid dynamic (CFD) thermohydrodynamic (THD) numerical simulations [27], the effect of nanoparticles on the performance characteristics of plain journal bearings is evaluated. Particularly, 3D simulation of a journal bearing is implemented using CFD which considerably improves the accuracy of results, coupled with conjugate heat transfer model for metal parts of bearings [28]. It is shown that the spatial temperature distribution in the lubricant film is accurately calculated. In this study, Reynolds equation model is used to calculate the oil-film pressure developed in hydrodynamic journal bearings by applying the nano-based lubricants.

The nanoparticle used for improving the lubricant is TiO_2. For evaluating the performance of this lubricant, different types of oils including DTE 24, DTE 25, and DTE 26 are considered. Moreover, the nanoparticle volume fractions of 0%, 5%, and 10% and rotational speeds of 500, 1000, and 1500 rev/min are examined to study the behavior of nanoparticle additive to the lubricant.

2. Mathematical Problem

The configuration of thrust bearing consists of six pads in this study. To ensure self-adjustment ability due to loading requirements, each pad is positioned between two grooves and is supported at a pivot point. The wedge-shaped geometry of the lubricant film constituted between the rotor and inclined pad results in pressure built-up. External thrust of the bearing is equal to the integration from such pressure built-up over the rotor surface. It is assumed that the thrust bearing works without misalignment (i.e., the main surfaces of the stator and rotor are considered parallel), while the sliding surface of the runner (collar) is supposed to be smooth and plane. Understanding symmetry in physical systems makes it easier to explain physical phenomena and leads to simplifications in the mathematical explanation of the nature of the problem. Because of the symmetrical geometry of this problem for the pads, simulation of a single pad is feasible with considering these assumptions instead of the entire domain resulting in substantial reduction of modeling complexity and computational cost.

Figure 1 represents the computational domain which contains the lubricant that is confined between the pad and collar and a single pad as the corresponding part of the collar. The problem is solved using CFD techniques for obtaining (a) pressure and temperature fields in the lubricant domain and (b) temperature fields of the pad and rotor, considering heat dissipation and conjugate heat transfer, respectively. In this model, cavitation effects are not taken into account in the lubricant domain, and negative values of oil pressure are neglected. Geometrical parameters of the present test-case is introduced in Table 1.

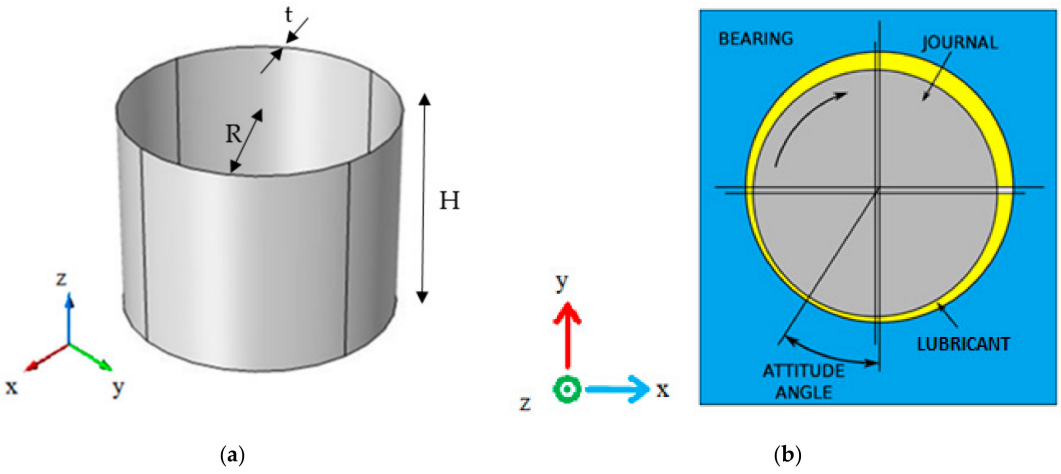

Figure 1. (**a**) Computational domain of oil film and (**b**) schematic of bearing, journal, and lubricant.

Table 1. Geometrical characteristics of the bearing.

Parameter	Value	Unit	Description
Number of pads	6	-	Number of pads
R	0.03	M	Journal radius
T	0.051	M	Solid thickness
H	0.05	M	Journal height
c	0.00003	M	Clearance between the journal and the bearing

2.1. Governing Equations

In this section, the equations governing the hydrodynamic lubrication of journal bearings are studied, taking into account the temperature effects and the characteristic parameters of this group of bearings.

The lubricant fluid used for this study is considered as Newtonian fluid [29]. The viscosity of Newtonian fluids is constant therefore, following equations can be used as governing equations [30]. The governing equations for a laminar steady-state incompressible flow in the absence of gravitational and external body forces can be written as:

$$\nabla.V = 0 \tag{1}$$

$$\rho(V.\nabla)V = -\nabla P + \nabla.(\mu \nabla V) \tag{2}$$

In the above equations, V is velocity vector, P is pressure, and μ is oil viscosity.

2.2. Lubricant Film Thickness in Bearings

Given the geometry of the journal bearings as shown in Figure 2, the thickness of the lubricant film can be calculated from Equation (3) in the space between the inner surface of bearing shell and the outer surface of rotary bearing.

$$h = C_m\left(1 - X_j \sin\theta - Y_j \cos\theta\right) \tag{3}$$

In Equation (3), h is gap function, C_m is the minimum radial clearance and it is defined when the bearing and the axis are centered. Parameters X_j and Y_j indicate the position of the journal center in the static equilibrium state (dimensionless) relative to the coordinate axes.

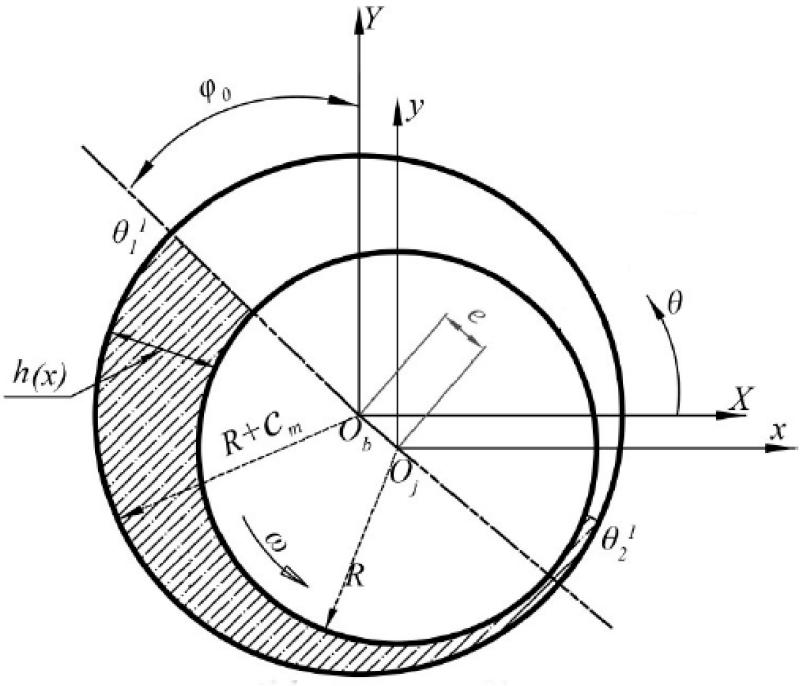

Figure 2. Schematic and parameters of circular hydrodynamic journal bearing.

2.3. Reynolds Equation

The Reynolds equation governing the hydrodynamic lubrication of finite length journal bearings by incompressible fluid in steady state is [31]:

$$\frac{\partial}{\partial x}\left(\frac{h^3}{\mu}\frac{\partial P}{\partial x}\right)+\frac{\partial}{\partial z}\left(\frac{h^3}{\mu}\frac{\partial P}{\partial z}\right)=6U\frac{\partial h}{\partial x} \tag{4}$$

In the above equation, μ is viscosity of the lubricant fluid, and U is linear velocity of the rigid rotor. By applying the rules of the generalized derivative interpolation method to Equation (4), the following equation is obtained at all stages of the evaluation regardless of the temperature effects and assuming the stability of the lubricant viscosity. The steady-state isothermal pressure distribution in the lubricant fluid film is achievable by solving Equation (5) [31].

$$\begin{gathered}\left(\frac{\partial h^3}{\partial x}\right)_i\sum_{k=1}^{N_x}A_{i,k}^{(1)}P_{k,j}+(h)_i^3\sum_{k=1}^{N_x}A_{i,k}^{(2)}P_{k,j}+(h)_i^3\sum_{l=1}^{N_y}B_{j,l}^{(2)}P_{i,l}=6\mu U\left(\frac{\partial h}{\partial x}\right)_i\\ i=1,2,\ldots,N_x \qquad j=1,2,\ldots,N_y\end{gathered} \tag{5}$$

where, the variables i and j refer to the location of the selected sample points (x_i, y_j) on the meshed domain of the problem as shown in Figure 3; N_x and N_y are the number of sampling points in the x and y directions of the field variable domain. Assuming the viscosity of the lubricant fluid to be varied in Equation (4) and re-applying the rules of the GDQ method, the following equation is derived to extract the values of thermal pressure created at different points of the lubricant fluid film:

$$\begin{gathered}\left(\frac{1}{\mu}\right)_{i,j}\left(\frac{\partial h^3}{\partial x}\right)\sum_{k=1}^{N_x}A_{i,k}^{(1)}P_{k,j}-\left(\frac{h^3}{\mu^2}\right)_{i,j}\sum_{k=1}^{N_x}A_{i,k}^{(1)}\mu_{k,j}\sum_{k=1}^{N_x}A_{i,k}^{(1)}P_{k,j}\\ +\left(\frac{h^3}{\mu}\right)_{i,j}\sum_{k=1}^{N_x}A_{i,k}^{(2)}P_{k,j}-\left(\frac{h^3}{\mu^2}\right)_{i,j}\sum_{l=1}^{N_y}B_{j,l}^{(1)}\mu_{i,l}\sum_{l=1}^{N_y}B_{j,l}^{(1)}P_{i,l}\\ +\left(\frac{h^3}{\mu}\right)_{i,j}\sum_{l=1}^{N_y}B_{j,l}^{(2)}P_{i,l}=6\mu U\left(\frac{\partial h}{\partial x}\right)_i\\ i=1,2,\ldots,N_x \qquad j=1,2,\ldots,N_y\end{gathered} \tag{6}$$

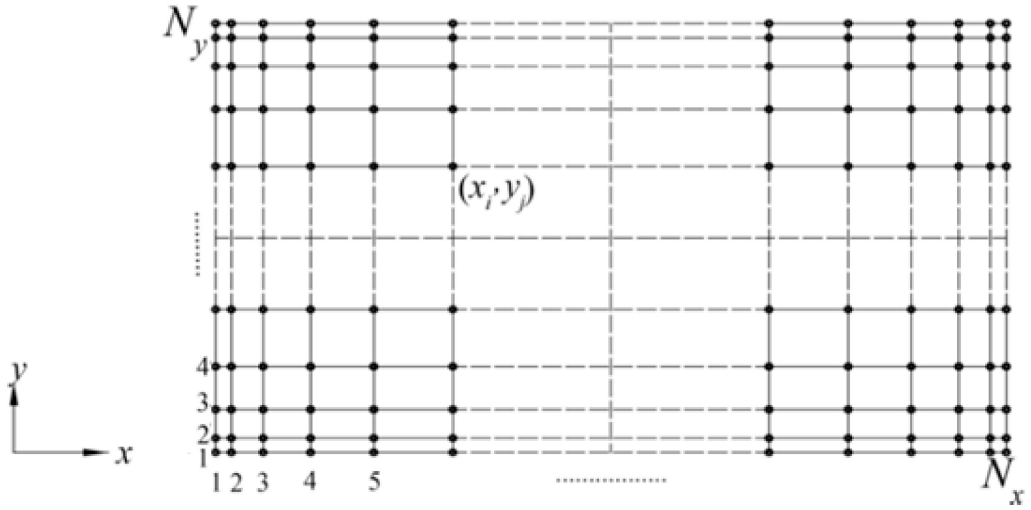

Figure 3. The position of sample nodes on the problem domain in order to determine the temperature and pressure distribution at different points of the lubricant film.

In Equations (5) and (6), P refers to the pressure created in the lubricant fluid film. Moreover, $A_{i,k}^{(1)}$ and $B_{j,l}^{(1)}$ represent the weight coefficients matrices for the first-order derivatives of the pressure distribution along the x and y axes, and $A_{i,k}^{(2)}$ and $B_{j,l}^{(2)}$ represent the second-order weight coefficients matrices for the P functions.

2.4. Thermophysical Properties

The monodispersed particle has no effect on the fluid flow field and its contributions on thermophysical properties were considered as described in Equations (7)–(10) [29] to change the rheology of the fluid.

$$\text{Density} \quad \rho_f = (1-\varphi)\rho_b + \varphi\rho_{sn} \tag{7}$$

$$\text{Heat capacity} \quad \left(\rho C_p\right)_f = (1-\varphi)\left(\rho C_p\right)_b + \varphi\left(\rho C_p\right)_{sn} \tag{8}$$

$$\text{Dynamic viscosity} \quad \mu_f = \frac{\mu_b}{(1-\varphi)^{2.5}} \tag{9}$$

$$\text{Thermal conductivity} \quad \lambda_f = \lambda_b \frac{\lambda_{sn} + 2\lambda_b - 2\varphi(\lambda_b - \lambda_{sn})}{\lambda_{sn} + 2\lambda_b + \varphi(\lambda_b - \lambda_{sn})} \tag{10}$$

In the above equations, φ is nanoparticle volume fraction, ρ is density, C_p is specific heat capacity, μ is dynamic viscosity, and λ is thermal conductivity. Subscripts b, sn, and f denote base fluid, solid nanoparticles, and nanofluid, respectively.

2.5. Energy Equation

Energy equation for fluid and solid domains are stated in Equations (11) and (12), respectively:

$$\rho C_{Pf} V.\nabla T = \nabla.\left(\lambda_f \nabla T\right) - \tau : \nabla V \tag{11}$$

$$\nabla.(\lambda_s \nabla T) = 0 \tag{12}$$

In the above equations, T is temperature, and τ is the viscous stress tensor. The subscripts f and s denote for oil, and pad and the rotor, respectively. Table 2 tabulates the thermophysical properties of lubricant and solid bearing body. The McCoull and Walther relation is applied to calculate the variation of viscosity with temperature [32]:

$$log\ (\nu + a) = b - n\ log(T) \tag{13}$$

Table 2. Thermophysical properties of the rotor and stator and the lubricant.

Lubricant	$\rho\left(kg/m^3\right)$	855
	$\lambda_f\left(\frac{W}{mK}\right)$	0.13
	$C_{Pf}\left(\frac{J}{kg\ K}\right)$	2035
Solid	$\rho_s\left(kg/m^3\right)$	7800
	$\lambda_s\left(\frac{W}{mK}\right)$	47
	$C_{Ps}\left(\frac{J}{kg\ K}\right)$	434

In the above equation, ν is the lubricant kinematic viscosity; a, b, and n are constant values equal to $a = 0.6$, $b = 9.51504$, and $n = 3.72684$ taken from the DTE 26.

The pad wall is considered to be stationary and angular velocity (ω) is assumed to be constant regarding the circumferential velocity at each local radius (r) which is equal to $U = \omega \cdot r$. Unless stated otherwise, no-slip conditions for fluid velocity are applied on the fluid-pad and fluid-collar

interfaces. Top and bottom edges of the pad are defined to be the oil inlet boundaries that have an oil pressure equal to 10 kPa above atmosphere. Temperature of the oil is specified by considering the hot-oil-carry-over effect that will be explored later. The film surface at the inner pad radius is assumed an opening (allowing both inflow and outflow): Pressure is presumed constant, with a specified value of 10 kPa. Fluid velocity and temperature respectively abide a zero normal gradient, $(\partial u/\partial n)_{r=R_i} = 0$, and Neumann boundary condition. The rest of fluid domain surfaces are taken as an outlet boundary condition considering a Neumann boundary condition for both temperature and velocity. Thermal outflow from the lubricant domain is only permitted.

Considering the thermal boundary conditions, a rotational periodicity condition is applied to the bearing solids and continuity of temperature and heat flux is assumed to be valid at the fluid–rotor and fluid–pad interfaces. Table 3 illustrates appropriate combinations of the convection coefficient, a_{conv}, and ambient temperature, T_{amb}, for the remaining external surfaces of the rotor and the pad.

Table 3. Thermal and flow boundary conditions for bearing of the present study.

Domain	Position	Boundary Condition
Pad		
	Top (Fluid-Solid interface)	Continuity of heat flux and temperature
	Bottom/ Outer surface/ Inner surface	$\begin{cases} a_{conv} = 100\ \frac{W}{m^2\ K} \\ T_{feed} = 50\ ^\circ C \\ Q_{feed} = 0.00025\ m^3/s \end{cases}$
	Inlet Side/Outlet Side	Adiabatic
Fluid		
	Inlet/Inner side	Zero relative pressure, $\frac{\partial V}{\partial n} = \frac{\partial T}{\partial n} = 0$
	Outer side/Outlet	Zero relative pressure, $\frac{\partial V}{\partial n} = \frac{\partial T}{\partial n} = 0$

It is essential to consider heat dissipation in the lubricant domain, convective heat transfer, conjugate heat transfer through solid domains of the bearing, besides oil mixing in the groove regions of the bearings, for an accurate determination of temperature distribution in the lubricant and solid domains. Particularly, heat produced in the lubricant because of viscous shear is partially released through the adjacent structure, but mostly is removed by the flow, and it will be discharged into a drain or cooling container. In theory, the outflow hot oil is substituted with the low temperature feeding oil. Still, the bearing pads are organized so that the preceding pad outlet is situated close to the following pad inlet, and the groove is minimized between pads to enhance the active bearing surface. Subsequently, warm lubricant exists in the spacing between pads, which also affects the inlet oil temperature.

In the current bearing arrangement, lubricating oil is fed into the lubricating region through six radial grooves from the bearing inner diameter. Subsequently, the hot-oil-carry-over effect is considered for determination of inlet oil temperature. Thus, from the equation of mass conservation for the lubricant film and the equation of energy conservation for a single groove, the following equations can be attained:

$$Q_{in} = Q_{or} + Q_{ex} + Q_{ir} \tag{14}$$

$$Q_{feed} = Q_{dr} + Q_{or} \tag{15}$$

$$Q_{feed}T_{feed} + Q_{ir}T_{ir} + Q_{ex}T_{ex} + H_{rotor} = (Q_{dr} + Q_{ir})T_{in} + H_{groove} \tag{16}$$

In the above equations, Q is flow rate demarcated by $feed$, ir, or, ex, and dr subscripts to denote feeding oil, inner bearing surface, outer bearing surface, outflow bearing surface, and from the outer radius of the groove region, respectively. Considering relevant assumptions in the groove region, the

amount of heat from the collar is considered to be equal to the amount absorbed heat by the bearing housing; therefore, H_{rotor} and H_{groove} can be ignored. By the combination of Equations (14)–(16), the following equation can be derived, which will be utilized for determination of the inlet oil temperature:

$$T_{in} = \frac{Q_{feed}T_{feed} + Q_{ir}T_{ir} + Q_{ex}T_{ex}}{Q_{feed} + Q_{ir} + Q_{ex}} \tag{17}$$

For hydrophobic surfaces, the no-slip condition cannot be assumed for the fluid-solid interface. In this research, based on the modified Navier model [33], it is presumed that the fluid and surface velocities at the hydrophobic boundary vary. The velocity difference between the wall and fluid particles at the wall-fluid interface is imposed at the hydrophobic boundaries while solving the Navier-Stokes equations. In the modified Navier model, slip condition occurs when local shear stress exceeds a critical value, τ_{cr}, and fluid slip velocity can be obtained as:

$$u_s = \begin{cases} 0 & \tau < \tau_{cr} \\ (\tau - \tau_{cr})\frac{b}{\eta} & \tau \geq \tau_{cr} \end{cases} \tag{18}$$

where τ_{cr} is critical shear stress; it is defined as the wall shear stress where the slip begins and b is slip length; it is a surface property, showing how slippery it is when interacting with a specific fluid. In this research, τ_{cr} is presumed to be zero; hence, any non-zero shear stress condition at a hydrophobic boundary would start fluid slip. A 20 μm reference minimum film thickness value is assumed.

3. Numerical Algorithm

Equations (1)–(18) are solved by use of finite element method to model the problem. The method (3×3 Newton-Raphson) requires that the geometry/mesh is reconstructed in each iteration, and CFD solution is repeated until the final equilibrium is reached [34]. Figure 4 represents the simulation domain for two coarse and fine meshes.

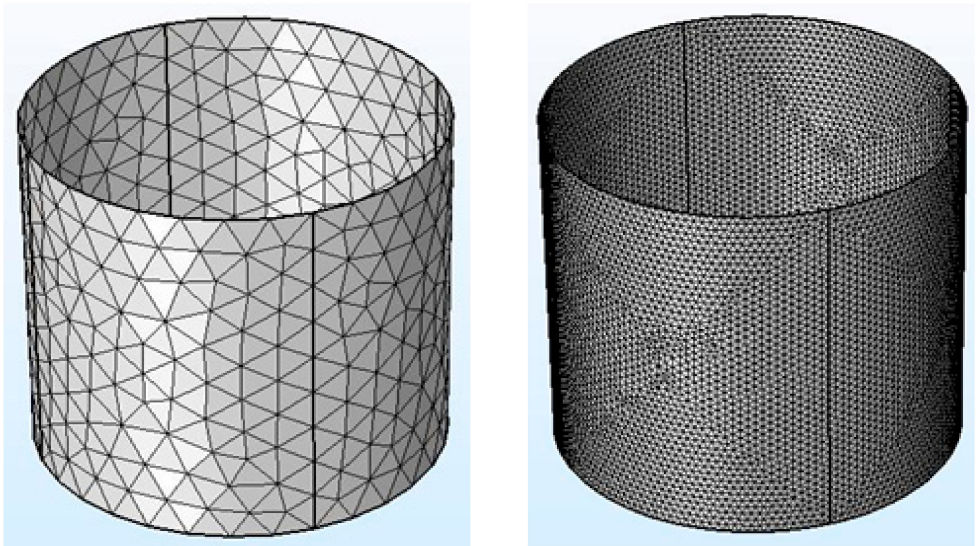

(**a**) (**b**)

Figure 4. Various meshes used for grid study (**a**) coarse mesh (**b**) fine mesh.

In order to validate the results in the following section and check the dependency of numerical results to the mesh resolution, the lowest film pressure profile is measured for six different mesh resolutions which are defined in Table 4. The number of meshes varies from 64 to 16,212 elements for different resolutions of meshes.

Table 4. Different mesh resolution and correspondence relative error percentage with respect to exact solution.

Mesh Resolution	Number of Elements	Relative Percent Error in Pressure Calculation
Coarser	64	183.22
Coarse	276	78.4
Normal	812	18.66
Fine	1180	2.17
Finer	5724	0.53
Extremely fine (Exact)	16,212	0

For evaluating the precision of the meshes, an extremely fine mesh with 16,212 elements is implemented and is considered as an exact solution. The percentage of error for other meshes are calculated compared to this solution. The results of the lowest film pressure profile for various mesh sizes are illustrated in Figure 5 and the error percentages are presented in Table 4.

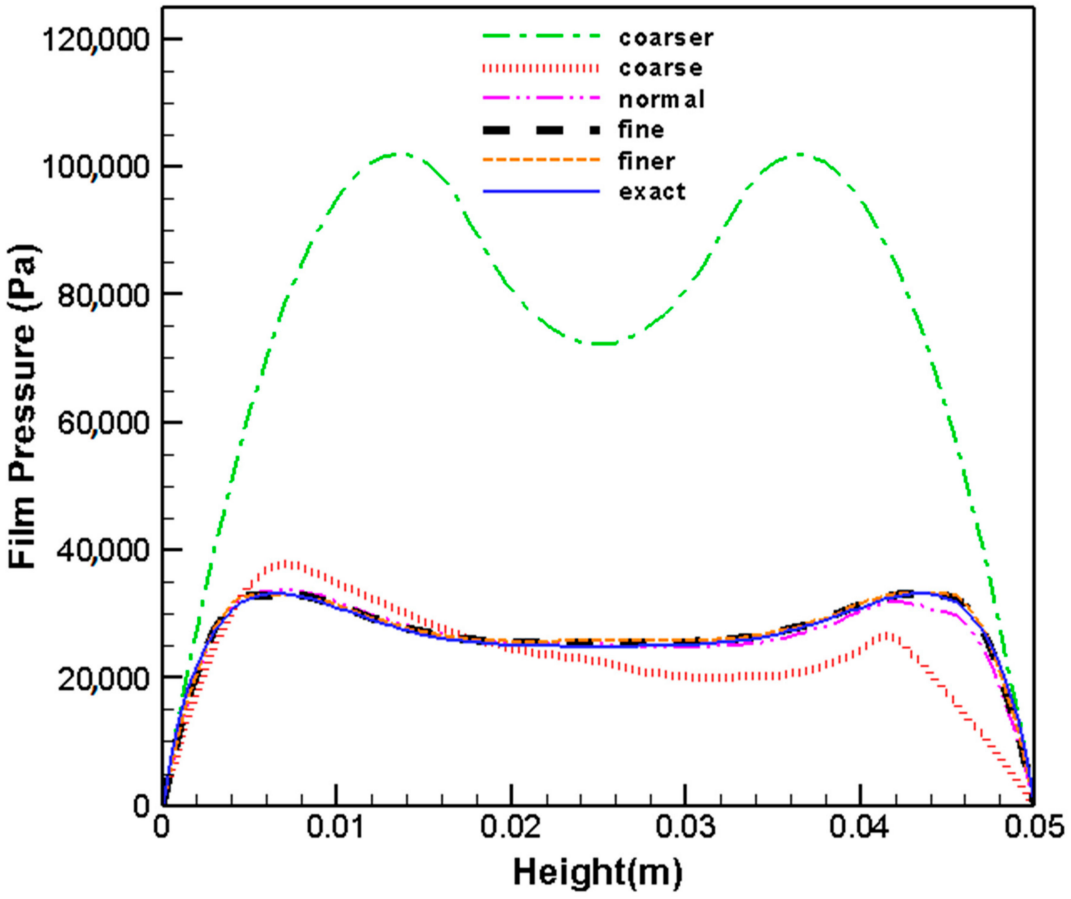

Figure 5. Comparison of film pressure profile along the longitudinal line for various mesh sizes.

The results show that the coarser mesh overestimates the lowest film pressure. The coarse mesh is not very accurate in terms of the results provided. However, the fine mesh produces accurate numerical results which is not very distinctive with the exact solution. Thus, the results with the fine mesh resolution will be used for numerical simulations.

4. Results and Discussions

The primary benefit of the pivoted-pad thrust bearings is their capability of providing superior performance over an extensive range of loads and rotational speeds. In this study, the effect of various

factors including rotational speed, nano particle volume fraction, and lubricant types on the journal bearing design performance are investigated. For evaluating the journal bearing performance, various parameters including fluid temperature on the bearing surface, pressure distribution, velocity vector, gap height between the bearing and journal surface, shear stress, dissipation power, and temperature rise are examined. In this study, TiO_2 is added to enhance the performance of the lubricant.

Figure 6 represents the fluid temperature on the bearing surface for the test cases under 7 kN specific loading, rotating at 1500 rpm speed with 10% of nanoparticle volume fraction. The figure clearly illustrates that the temperature monotonically increases along the z coordinate showing a variation of above 50 °C.

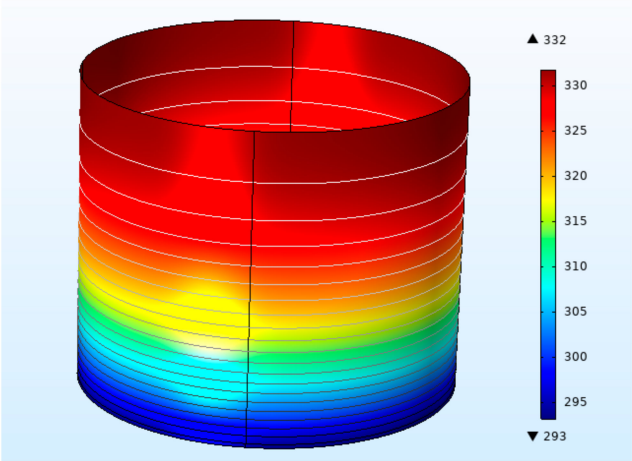

Figure 6. Fluid temperature in degree Celsius versus spatial position on the bearing surface for the test-case under 7 kN specific loading, rotating at 1500 rpm with 10% of nanoparticle volume fraction in DTE 26.

Figure 7 represents the pressure contours on the bearing surface for the test-case under 7 kN specific load at 1500 rpm rotational speed with 10% of nanoparticle volume fraction. The pressure contours are shown in both cylindrical arrangement (Figure 7a) and extended 2D view (Figure 7b). It is observed that the maximum and minimum pressure points are located at the middle cylinder. It is also observed that these maximum and minimum pressure points are adjacent to each other.

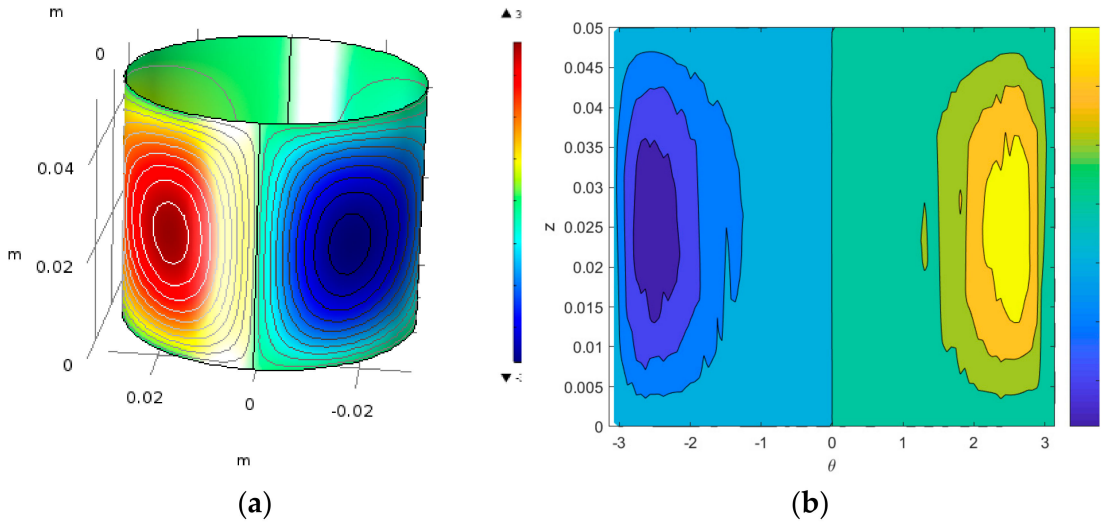

Figure 7. Pressure contours on the (**a**) cylindrical view and (**b**) extended two-dimensional (2D) planar view on the bearing surface for the test-case under 7 kN specific loading, rotating at 1500 rpm with 10% of nanoparticle volume fraction in DTE 26.

The velocity vectors are represented on the bearing surface for the test-case under 7 kN specific load at 1500 rpm rotational speed with 10% of nanoparticle volume fraction in Figure 8. It shows a uniform distribution of velocity vectors both in magnitude and direction while the rotation is on the counter clock-wise direction.

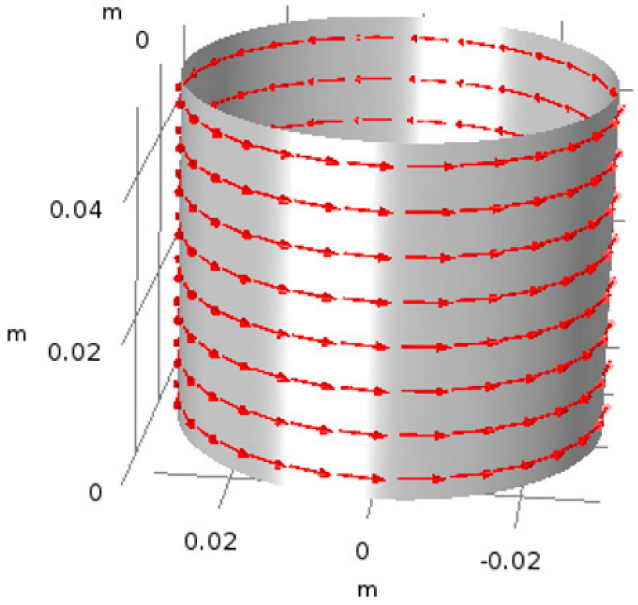

Figure 8. Velocity vectors on the bearing surface for the test-case under 7 kN specific loading, rotating at 1500 rpm with 10% of nanoparticle volume fraction in DTE 26.

Figure 9 shows the total gap height between the bearing and journal for the test-case under 7 kN specific loading, rotating at 1500 rpm with 10% of nanoparticle volume fraction. This figure indicates that the total gap height is constant along the z coordinate for a specific position on the cylindrical coordinate due to a uniform distribution of specific load. Moreover, it is observed that the maximum gap height is located on the plane passing the origin along the x axis with the value of 48 microns. The minimum value of total gap height is 12 micrometers located at opposite to the maximum point.

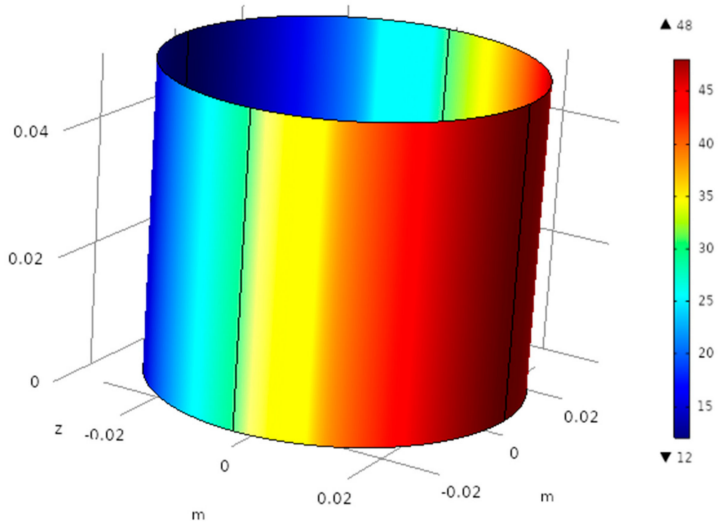

Figure 9. Total gap height in micrometers between the bearing and journal surface for the test-case under 7 kN specific loading, rotating at 1500 rpm with 10% of nanoparticle volume fraction in DTE 26.

Figure 10 represents the average shear stress ($\tau = \mu \frac{\partial U}{\partial r}$) variations as a function of rotational speed for different nanoparticle (TiO_2) volume fraction percentage and lubricant types. As DTE 26 lubricant has higher viscosity compared to the other two lubricants, the average shear stress for this lubricant is much higher. It is clearly observed that the average shear stress has a monotonic increasing trend in all cases. Moreover, the increasing trend is a linear function of rotational speed increments. It can be observed that for all different lubricant types, the rotational speed has a direct relationship with the increase of average shear stress. By increasing the rotational speed from 500 to 1500 rpm, the average shear stress increases by more than 100% for the DTE 26 lubricant type. This criteria is even higher for other lubricant types indicating slightly more than 120% and 130% increment for DTE 25 and DTE 24 lubricant types, respectively. Despite showing different values, increasing nanoparticles increases the average shear rate by approximately 10% for all cases. That is clearly observed since at higher nanoparticle volume fractions, the inter-particle interactions result in higher shear stress values.

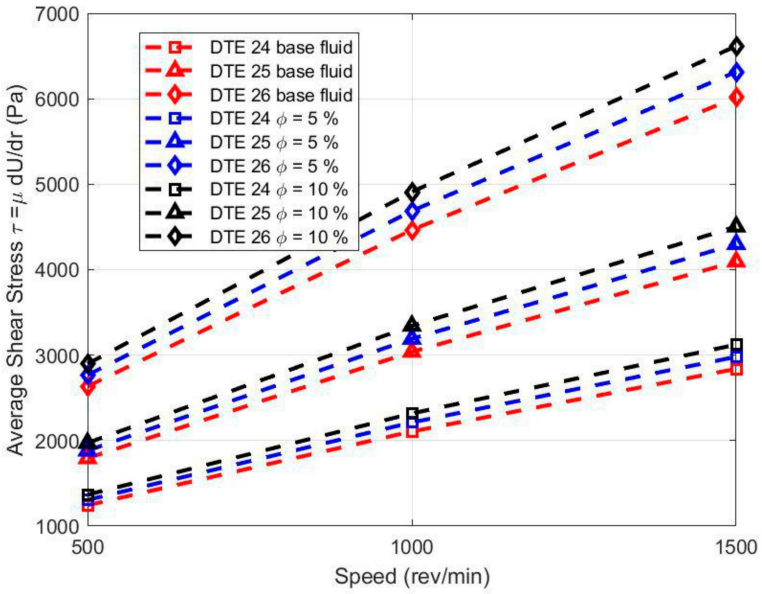

Figure 10. Variation in average shear stress as a function of rotational speed for different nanoparticle (TiO_2) volume fraction percentage and lubricant types; the test-case is simulated under 7 kN specific load.

Figure 11 illustrates the variations of dissipation power as a function of rotational speed for different nanoparticle (TiO_2) volume fraction percentage and lubricant types. The dissipation power also increases monotonically with the increment of rotational speed, but it shows an exponential trend in contrast to that of average shear stress. Similar to the previous figure, the rotational speed has a direct increasing relationship with the dissipation power. The increase rate is found to be much higher than that of the average shear stress showing an increase in the order of approximately 600% from 500 to 1500 rpm for the DTE 26 lubricant type. The increase rate is almost similar for different lubricant types, in contrast to what is observed for the average shear stress. Similar to what is observed in Figure 10, increasing nanoparticles volume fraction increases the average shear rate by approximately 10% for all lubricant types and in all rotational speeds.

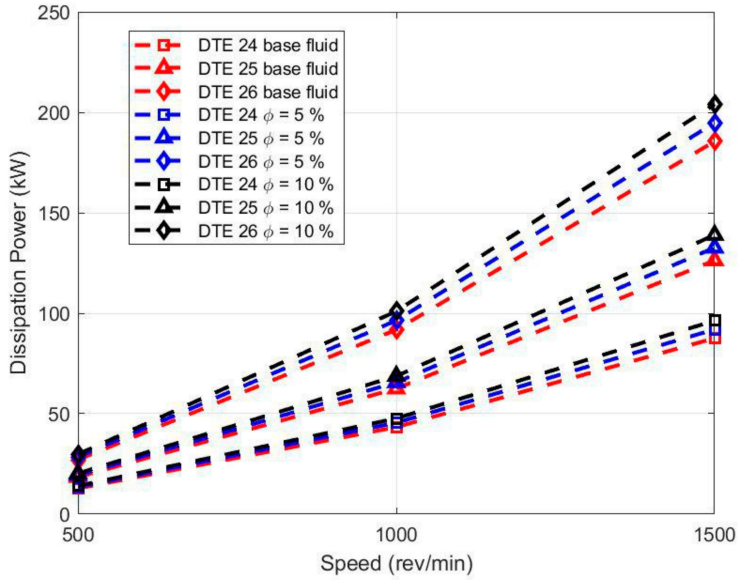

Figure 11. Variation in dissipation power in kW as a function of rotational speed for different nanoparticle (TiO_2) volume fraction percentage and lubricant types; the test-case is simulated under 7 kN specific load.

The temperature rise in a journal bearing affects the lubricant properties and performance of the system. The variations of temperature rise as a function of rotational speed for different nanoparticle (TiO_2) volume fraction percentage and lubricant types are shown in Figure 12. This figure shows an exponential trend for the increase of temperature as the rotational speed increases. This can be quantified by approximately 800% factor of increase from 500 to 1500 rpm for the DTE 26 lubricant type. The increase rate is almost similar for different lubricant types, in contrast to what is observed for the average shear stress.

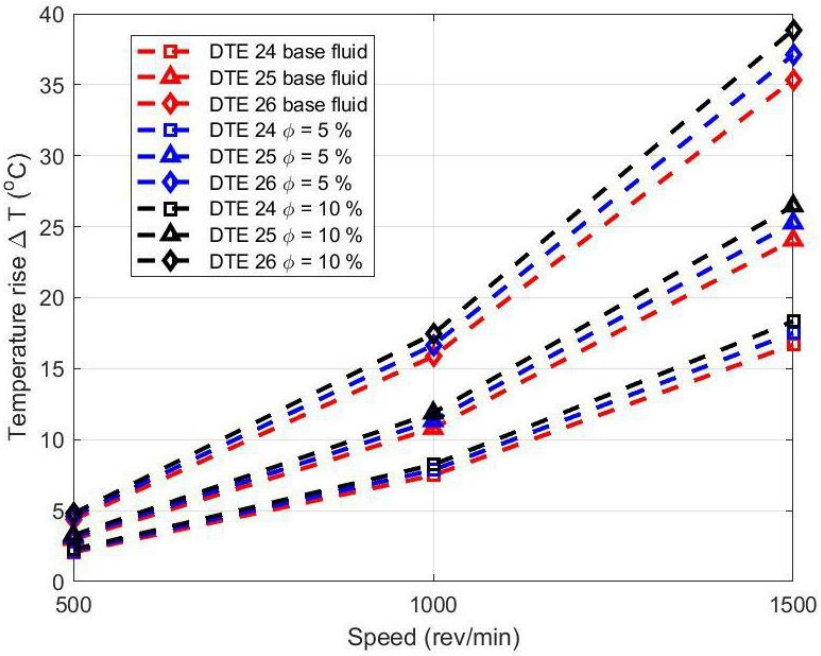

Figure 12. Variation in temperature rise with and without nanoparticles (TiO_2) in the lubricant.

5. Conclusions

In the present study, the effect of various factors including rotational speed, nanoparticle volume fraction, and lubricant types on the journal bearing design performance are investigated. For evaluating the journal bearing performance, various parameters including fluid temperature on the bearing surface, pressure distribution, velocity vector, gap height between the bearing and journal surface, shear stress, dissipation power, and temperature rise are examined. This will lead to achieving a correlation of data for installations of bearing. This will be very helpful in cases that parameters affecting the bearing operation cannot be easily specified. In order to achieve this goal, the Reynolds and energy equations governing the incompressible lubricating fluid flow have been solved in different steps. The following can be deduced from results of the present study:

- Temperature on the bearing surface increases monotonically along the z coordinate under specific loading.
- Maximum and minimum pressure on the bearing surface under specific loading is occurred at the middle cylinder. Moreover, these maximum and minimum pressure points are adjacent to each other.
- Distribution of velocity vectors under specific loading is uniform both in magnitude and direction while the rotation is on the counter clock-wise direction.
- Total gap height between the bearing and journal surface is constant along the z coordinate for a specific position on the cylindrical coordinate due to uniform distribution of specific load.
- For all different lubricant types, the rotational speed has a direct relationship with the increase of the average shear stress. By increasing the rotational speed from 500 to 1500 rpm, the average shear stress increases by more than 100%, 120%, and 130% for DTE 26, DTE 25, and DTE 24 lubricant types, respectively. Increasing nanoparticles enhances the average shear rate by approximately 10% for all cases.
- Dissipation power increases with the rotational speed. By increasing the rotational speed from 500 to 1500 rpm, average shear stress increases around 600% for all lubricant types. Increasing nanoparticles volume fraction increases the average shear rate by approximately 10% for all lubricant types and in all rotational speeds.
- By increasing the rotational speed from 500 to 1500 rpm, the temperature rise increases around 800% for almost all lubricant types.

Author Contributions: Conceptualization, M.Y.A.J.; methodology, M.Y.A.J.; software, M.Y.A.J.; validation, M.Y.A.J.; formal analysis, M.Y.A.J., R.A.; investigation, M.Y.A.J., R.A.; resources, M.Y.A.J.; data curation, M.Y.A.J., R.A.; writing—original draft preparation, R.A., writing—review and editing, W.-M.Y., L.K.B.L., S.L.; visualization, M.Y.A.J.; supervision, M.S.S.; project administration, M.Y.A.J., M.S.S.; funding acquisition, M.Y.A.J.

Funding: This research received no external funding.

Conflicts of Interest: The authors declare no conflicts of interest.

Nomenclature

R	Journal radius, **m**	N_x	Number of sampling points in the x direction
t	Solid thickness, m	N_y	Number of sampling points in the y direction
H	Journal height, m	Q	Flow rate, $m^3\ s^{-1}$
c	Clearance between the journal and the bearing, m	u_s	Slip velocity, m s^{-1}
φ	Nanoparticle volume fraction	λ	Thermal conductivity, $Wm^{-1}\ K^{-1}$
V	Fluid velocity vector, m s^{-1}	ν	Kinematic viscosity, cSt
P	Pressure, Pa	T	Temperature, K
μ	Dynamic viscosity, kg $m^{-1}s^{-1}$	τ	Viscous stress tensor, Pa
h	Gap function, m	a_{conv}	Convection coefficient, $Wm^{-2}\ K^{-1}$
C_m	Minimum radial clearance	T_{amb}	Ambient temperature, K
X_j	Position of the journal center in the static equilibrium state	Subscripts	
Y_j	Position of the journal center in the static equilibrium state	b	Base fluid
C_P	Specific heat capacity, J $kg^{-1}K^{-1}$	sn	Solid nanoparticles,
ω	Rotor angular velocity, rad s^{-1}	f	Fluid (oil)
U	Linear velocity of the rigid rotor, m s^{-1}	s	Solid (pad and rotor)
$A_{i,k}^{(1)}$	Weight coefficients matrices for the first-order derivatives of the pressure distribution	$feed$	Feeding oil
$B_{j,l}^{(1)}$	Weight coefficients matrices for the first-order derivatives of the pressure distribution	ir	Inner bearing surface
$A_{i,k}^{(2)}$	Second-order weight coefficients matrices for the pressure distribution	or	Outer bearing surface
$B_{j,l}^{(2)}$	Second-order weight coefficients matrices for the pressure distribution	ex	Outflow bearing surface
ρ	Density, kg m^{-3}	dr	Outer radius of the groove region
C_P	Specific heat capacity, J $kg^{-1}K^{-1}$	in	Inlet
b	Slip length, m	cr	Critical

References

1. Nguyen, T.; Tran, T.; de Boer, H.; van den Berg, A.; Eijkel, J.C.T. Rotary-Atomizer Electric Power Generator. *Phys. Rev. Appl.* **2015**, *3*, 034005. [CrossRef]
2. Nguyen, M.Q.; Shadloo, M.S.; Hadjadj, A.; Lebon, B.; Peixinho, J. Perturbation threshold and hysteresis associated with the transition to turbulence in sudden expansion pipe flow. *Int. J. Heat Fluid Flow* **2019**, *76*, 187–196. [CrossRef]
3. Shadloo, M.; Hadjadj, A. Laminar-turbulent transition in supersonic boundary layers with surface heat transfer: A numerical study. *Numer. Heat Transf. A* **2017**, *72*, 40–53. [CrossRef]
4. Crosby, W. Thermal considerations in the solution of finite journal bearings. *Wear* **1980**, *64*, 15–32. [CrossRef]
5. Nagaraju, Y.; Joy, M.; Nair, K.P. Thermohydrodynamic analysis of a two-lobe journal bearing. *Int. J. Mech. Sci.* **1994**, *36*, 209–217. [CrossRef]
6. Ma, M.T.; Taylor, C.M. An experimental investigation of thermal effects in circular and elliptical plain journal bearings. *Tribol. Int.* **1996**, *29*, 19–26. [CrossRef]
7. Banwait, S.; Chandrawat, H. Effect of misalignment on thermohydrodynamic analysis of elliptical journal bearings. *J. Inst. Eng. India Mech. Eng. Div.* **2000**, 93–101.
8. Singh, D.; Majumdar, B. Computer-aided design of hydrodynamic journal bearings considering thermal effects. *Proc. Inst. Mech. Eng. J* **2005**, *219*, 133–139. [CrossRef]
9. Mishra, P.; Pandey, R.; Athre, K. Temperature profile of an elliptic bore journal bearing. *Tribol. Int.* **2007**, *40*, 453–458. [CrossRef]

10. Chauhan, A.; Sehgal, R.; Sharma, R.K. Thermohydrodynamic analysis of elliptical journal bearing with different grade oils. *Tribol. Int.* **2010**, *43*, 1970–1977. [CrossRef]
11. Prasad, E.S.; Nagaraju, T.; Sagar, J.P. Thermohydrodynamic performance of a journal bearing with 3D-surface roughness and fluid inertia effects. *Int. J. Appl. Res. Mech. Eng.* **2012**, *2*, 18–24.
12. Singla, A.; Kumar, A.; Bala, S.; Singh, P.; Chauhan, A. Thermo-hydrodynamic Analysis on Temperature Profile of Circular Journal Bearing Using Computational Fluid Dynamics. In Proceedings of the 2014 Recent Advances in Engineering and Computational Sciences, Chandigarh, India, 6–8 March 2014; pp. 1–6.
13. Baskar, S.; Sriram, G.; Arumugam, S. The Use of D-optimal Design for Modeling and Analyzing the Tribological Characteristics of Journal Bearing Materials Lubricated by Nano-Based Biolubricants. *Tribol. Trans.* **2016**, *59*, 44–54. [CrossRef]
14. Solghar, A.A. Investigation of nanoparticle additive impacts on thermohydrodynamic characteristics of journal bearings. *Proc. Inst. Mech. Eng. J* **2015**, *229*, 1176–1186. [CrossRef]
15. Li, X.; Zhu, D.; Wang, X. Experimental investigation on viscosity of Cu-H_2O nanofluids. *J. Wuhan Univ. Technol.-Mater. Sci. Ed.* **2009**, *24*, 48–52. [CrossRef]
16. Abdollahzadeh Jamalabadi, M.Y.; Ghasemi, M.; Alamian, R.; Wongwises, S.; Afrand, M.; Shadloo, M.S. Modeling of Subcooled Flow Boiling with Nanoparticles under the Influence of a Magnetic Field. *Symmetry* **2019**, *11*, 1275. [CrossRef]
17. Pordanjani, A.H.; Aghakhani, S.; Afrand, M.; Mahmoudi, B.; Mahian, O.; Wongwises, S. An updated review on application of nanofluids in heat exchangers for saving energy. *Energy Convers. Manag.* **2019**, *198*, 111886. [CrossRef]
18. Rejvani, M.; Saedodin, S.; Vahedi, S.M.; Wongwises, S.; Chamkha, A.J. Experimental investigation of hybrid nano-lubricant for rheological and thermal engineering applications. *J. Therm. Anal. Calorim.* **2019**, *138*, 1823–1839. [CrossRef]
19. Asadi, A.; Aberoumand, S.; Moradikazerouni, A.; Pourfattah, F.; Żyła, G.; Estelle, P.; Mahian, O.; Wongwises, S.; Nguyen, H.M.; Arabkoohsar, A. Recent advances in preparation methods and thermophysical properties of oil-based nanofluids: A state-of-the-art review. *Powder Technol.* **2019**, *352*, 209–226. [CrossRef]
20. Suryawanshi, S.; Pattiwar, J. Effect of TiO2 Nanoparticles Blended with Lubricating Oil on the Tribological Performance of the Journal Bearing. *Tribol. Ind.* **2018**, *40*, 370–391. [CrossRef]
21. Lee, C.-G.; Hwang, Y.-J.; Choi, Y.-M.; Lee, J.-K.; Choi, C.; Oh, J.-M. A study on the tribological characteristics of graphite nano lubricants. *Int. J. Precis. Eng. Manuf.* **2009**, *10*, 85–90. [CrossRef]
22. Tao, Y.; Tao, Y.; Wang, B.; Tai, Y. Preparation and investigation of nano-AlN lubricant with high performance. *Mater. Chem. Phys.* **2014**, *147*, 28–34. [CrossRef]
23. Binu, K.; Shenoy, B.; Rao, D.; Pai, R. A variable viscosity approach for the evaluation of load carrying capacity of oil lubricated journal bearing with TiO2 nanoparticles as lubricant additives. *Procedia Mater. Sci.* **2014**, *6*, 1051–1067. [CrossRef]
24. Binu, K.; Shenoy, B.; Rao, D.; Pai, R. Static characteristics of a fluid film bearing with TiO2 based nanolubricant using the modified Krieger–Dougherty viscosity model and couple stress model. *Tribol. Int.* **2014**, *75*, 69–79. [CrossRef]
25. Babu, K.S.; Nair, K.P.; Rajendrakumar, P. Computational analysis of journal bearing operating under lubricant containing Al 2 O 3 and ZnO nanoparticles. *Int. J. Eng. Sci. Technol.* **2014**, *6*, 34–42. [CrossRef]
26. Jatti, V.S.; Singh, T. Copper oxide nano-particles as friction-reduction and anti-wear additives in lubricating oil. *J. Mech. Sci. Technol.* **2015**, *29*, 793–798. [CrossRef]
27. Papadopoulos, C.; Kaiktsis, L.; Fillon, M. CFD thermohydrodynamic analysis of 3-D sector-pad thrust bearings with rectangular dimples. In Proceedings of the ASME Turbo Expo 2013: Turbine Technical Conference and Exposition, San Antonio, TX, USA, 3–7 June 2013.
28. Jamalabadi, M.Y.A. Effects of Nanoparticle Enhanced Lubricant Films in Dynamic Properties of Plain Journal Bearings at High Reynolds Numbers. *Int. J. Eng. Technol.* **2017**, *13*, 1–23. [CrossRef]
29. Hatami, M.; Ganji, D.D.; Sheikholeslami, M. Chapter 3—DTM for Heat Transfer Problems. In *Differential Transformation Method for Mechanical Engineering Problems*; Hatami, M., Ganji, D.D., Sheikholeslami, M., Eds.; Academic Press: London, UK, 2017; pp. 103–151.
30. Nguyen, T.; van der Meer, D.; van den Berg, A.; Eijkel, J.C. Investigation of the effects of time periodic pressure and potential gradients on viscoelastic fluid flow in circular narrow confinements. *Microfluid. Nanofluid.* **2017**, *21*, 37. [CrossRef]

31. Rahmatabadi, A.; Mehrjardi, M.Z.; Fazel, M. Performance analysis of micropolar lubricated journal bearings using GDQ method. *Tribol. Int.* **2010**, *43*, 2000–2009. [CrossRef]
32. Frene, J.; Nicolas, D.; Degueurce, B.; Berthe, D.; Godet, M. *Hydrodynamic Lubrication: Bearings and Thrust Bearings*; Elsevier: Amsterdam, The Netherlands, 1997; Volume 33.
33. Spikes, H.; Granick, S. Equation for slip of simple liquids at smooth solid surfaces. *Langmuir* **2003**, *19*, 5065–5071. [CrossRef]
34. Shadloo, M.S. Numerical Simulation of Compressible Flows by Lattice Boltzmann Method. *Numer. Heat Transf. A* **2019**, *75*, 167–182. [CrossRef]